IEEE Access
Multidisciplinary ⋮ Rapid Review ⋮ Open Access Journal

Received May 10, 2022, accepted May 23, 2022, date of publication May 26, 2022, date of current version June 1, 2022.

*Digital Object Identifier 10.1109/ACCESS.2022.3178135*

# Coordinated Compensation Between Active and Semi-Active Actuators for Suspension Control System

**YONGHWAN JEONG[1], YOUNGIL SOHN[2], SEHYUN CHANG[2], AND SEONGJIN YIM[1], (Member, IEEE)**

[1]Department of Mechanical and Automotive Engineering, Seoul National University of Science and Technology, Nowon-gu, Seoul 01811, Republic of Korea
[2]Institute of Advanced Technology Development, Hyundai Motor Company, Seongnam-si, Gyeonggi-do 13529, Republic of Korea

Corresponding author: Seongjin Yim (acebtif@seoultech.ac.kr)

This work was supported by the Research Program through Hyundai Motor Group.

**ABSTRACT** This paper presents coordinated compensation schemes between active and semi-active actuators in suspension control system. Generally in active suspension systems, active actuators have been adopted to generate a control force calculated by a controller. However, active actuators adopted in actual vehicles have physical constraints such as maximum force, bandwidth and force-velocity limitation. On the other hand, a semi-active actuator can be a good alternative to active one in view of maximum force and bandwidth despite it cannot generate an active control force. However, the performance of semi-active actuators is limited by half of active ones. Hence, it is necessary to compensate the control force of semi-active actuators by active ones. In this paper, it is assumed that a vehicle has both of active and semi-active actuators. A control force needed to enhance ride comfort is generated by linear quadratic regulator (LQR). The controller is designed with 2-DOF quarter-car model and applied into 7-DOF full-car one. To generate the control force with active and semi-active actuators, several coordinated compensation schemes are proposed. A simulation on a simulation package show that the proposed coordinated compensation schemes are effective in reducing the control force of the active actuator over the wider range of frequencies.

**INDEX TERMS** Active suspension, coordinated control, LQR, LQ SOF control, semi-active suspension.

## I. INTRODUCTION

The objectives of the suspension system design are classified into two categories: ride comfort and road holding. Generally, three measures, vertical acceleration of a sprung mass, suspension stroke, and tire deflection, are typically used to evaluate the suspension system in terms of these objectives [1]. The vertical acceleration of a sprung mass is the key measure to assess the ride comfort of the suspension system. Effects of the vertical acceleration on passengers are evaluated by using the international standard, ISO 2631-1, which defined the sensitivity of the human body to vibration [2], [3]. Road holding is assessed with the suspension stroke and the tire deflection. The relationship between two objectives and three measures has been summarized in the literature [4], [5].

The associate editor coordinating the review of this manuscript and approving it for publication was Ton Duc Do.

Up to date, a lot of research papers on suspension control systems have been published [6]–[9]. According to the literature on suspension control, it can be assumed that a suspension control system has two-level structure: upper- and lower-level controllers [10]–[12]. An upper-level controller calculates a control force needed to improve ride comfort or road holding with controller design methodologies. A lower-level controller tries to generate an actual force calculated from the upper-level one with some actuators. If there is a single actuator, this is a reference or force tracking problem. If there are multiple actuators, this is a control allocation problem [13].

According to the two-level structure of a suspension control system, there are two research directions along the upper- and lower-level controllers in the literature. The research direction in the upper-level controller is controller design, which is to propose new controller design methodologies or to add several physical constraints exist in actual control system

to previously proposed methodologies. Several controller design methodologies such as LQR [14], LQ static output feedback control [15], [16], $H_\infty$ control [17], [18], fuzzy control [19], [20], adaptive control [21], [22], back-stepping control [23], [24] and model predictive control (MPC) [25], [26] have been proposed and applied in this direction. In these works, a lower-level controller has not been adopted under the assumption that an actuator has infinite bandwidth and can generate an unbounded control force. Some constraints such as actuator saturation, control input delay, actuator bandwidth and suspension travel limit have been taken into account in controller design stage [14], [18], [21]–[24], [26]. Among the controller design methodologies, MPC is the most applicable because it can explicitly handle the actuator constraints in spite of a large amount of its computational burden [25], [26]. Most of studies in this direction have done a simulation to verify the performance of proposed controllers.

The research direction in the lower-level controller is to design a force tracking controller with dynamic models of an actuator or to do experimental investigation [27]–[32]. In these works, a dynamic model on an actuator was derived and a force tracking controller is designed with it. For example, a hydraulic power unit and MR damper were modelled with a hydraulic circuit diagram and a Bouc-Wen model, respectively [27], [29]. Some papers have done experimental investigation with a particular actual actuator [33]–[38]. This paper concentrates on the lower-level controller.

Most of papers published up to date for suspension control have used a single actuator, i.e., active or semi-active actuator. As mentioned earlier, this is a reference tracking problem if there is a single actuator. On the other hand, there have been a little approaches to simultaneously use multiple actuators, i.e., active and semi-active one, for a suspension control system. Low bandwidth active suspension control with continuously variable damper were integrated to generate a control force [39]. Optimal control allocation was proposed to coordinate active and semi-active actuators [40]. In the work, quadratic programming was applied in control allocation stage. Hybrid suspension system was used to generate a control force given by filtered-X LMS and $H_\infty$ controllers [41], [42]. Different from the normal configuration that a spring, a damper and an active actuator are connected parallel to one another, the active actuator was serially connected to a spring and these were parallel to a semi-active actuator in the literature. Distribution of control force into these actuators was done by a dynamic optimal division. However, in the papers, actuator constraints were not explicitly handled. Another type of hybrid suspension, called hybrid electromagnetic active suspension (HEMAS), was proposed to utilize a linear actuator and MR damper which are connected parallel to each another [43]. In the work, the ideal force calculated from the upper-level controller was allocated into two actuators in the lower-level controller. However, an explicit allocation scheme was not presented in this paper. As for seat suspension of heavy-duty vehicles, the integrated active and semi-active control method was proposed [44]. This is a modified semi-active on-off control method with the compensation of small active force on the off-state of the MR damper. In other words, it is a sort of switching scheme between the active and semi-active actuators.

This paper uses active and semi-active actuators simultaneously to generate a control force, which is calculated from the upper-level controller. Generally, the control allocation converts the control force into the forces generated by several actuators. This is valid for the condition that each actuator can generate the control force. Let denote the area where an actuator can generate the control force with respect to velocity as the control area. Let denote the intersection of the control areas of several actuators as the common control area. As for a suspension control system with active and semi-active actuators, the common control area is small. In other words, the control areas of actuators are separated from each other. Under the condition, the control allocation is not effective. Instead of the control allocation, active and semi-active actuators can compensate drawbacks of each other under a particular rule [44]. Let denote this as the coordinated compensation.

For the coordinated compensation, this paper proposes two schemes between active and semi-active actuators: active-first and semi-active-first schemes. The active-first scheme uses an active actuator, which has several constraints such as force saturation, bandwidth and force-velocity limit. In this scheme, a semi-active actuator compensates a control force at high velocity where an active actuator cannot generate the force. Moreover, it can cover the saturation, i.e., the maximum force limitation of an active actuator. The semi-active-first scheme uses a semi-active actuator at 2 and 4 quadrants. In this scheme, an active actuator compensates a control force at 1 and 3 quadrants where a semi-active actuator cannot generate the force. This scheme is identical to that of the previous study [44].

The focus of this paper is not the control allocation but the coordinated compensation among multiple actuators. The coordinated compensation schemes proposed in this paper have several advantages over the suspension system with a single actuator. The first is that the limited performance of an active actuator due to several constraints can be compensated by a semi-active one. The second is that the energy consumption of an active actuator can be reduced by virtue of a semi-active actuator in case of the semi-active-first scheme. The third is that the most relevant scheme can be selected according to capacity of active and semi-active actuators. The fourth is that the control performance of the active-first scheme at high frequency can be improved by a semi-active actuator. To assess the effectiveness of the proposed coordinated compensation schemes, a simulation with the vehicle simulation package CarMaker is conducted. With simulation, four schemes, i.e., active-only, semi-active-only, active-first, semi-active-first schemes, are compared with one another.

This paper consists of four sections. In Section II, LQR is designed in the upper-level controller. In Section III,

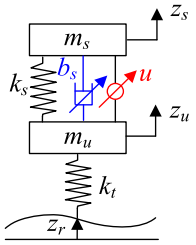


**FIGURE 1.** 2-DOF quarter-car model.

coordinated compensation schemes are presented. In Section IV, a simulation is conducted and simulation results are analyzed. The conclusions are given in Section V.

## II. DESIGN OF CONTROLLER FOR SUSPENSION

In this section, the upper-level controller is designed with LQR with a 2-DOF quarter-car model. The details of the 2-DOF quarter-car model are depicted in Fig. 1 [15], [16]. A vehicle is modeled as a sprung mass $m_s$ and unsprung mass $m_u$ to describe the vertical motions. The vertical displacements of $m_s$ and $m_u$ are defined as dynamic variables $z_s$ and $z_u$, respectively. As shown in Fig. 1, the active actuator is installed in parallel with the spring and damper. The road profile, $z_r$ is the disturbance of quarter-car model. In Fig. 1, the damper is a semi-active actuator with a particular damping curve. In controller design stage, it is assumed that the damper is linear and has constant damping coefficient, $b_s$.

In this paper, the suspension stroke and its rate are defined as $x$ and $v$, as given in (1). With these variables, the suspension force $f$ with control input $u$ between the sprung and unsprung masses is determined as (2). Based on the suspension force $f$ and dynamic variable $z_s$ and $z_u$, the equations of motion of the quarter-car model are derived as (3). Since the second order derivative of $z_s$ and $z_u$ are used in (3), not only the $z_s$ and $z_u$, but also the derivative of $z_s$ and $z_u$ are included to the state vector, as given in (4). With the equations of motion and the state vector, the state-space equation is derived as (5). The matrices $\mathbf{A}$, $\mathbf{B}_1$ and $\mathbf{B}_2$ are obtained as (6). The details of the derivation of state-space equation with the matrices $\mathbf{A}$, $\mathbf{B}_1$ and $\mathbf{B}_2$ can be found in [15].

$$\begin{cases} x = z_s - z_u \\ v = \dot{z}_s - \dot{z}_u \end{cases} \tag{1}$$

$$f = -k_s x - b_s v + u \tag{2}$$

$$\begin{cases} m_s \ddot{z}_s = f \\ m_u \ddot{z}_u = -f - k_t (z_u - z_r) \end{cases} \tag{3}$$

$$x = \begin{bmatrix} z_s & z_u & \dot{z}_s & \dot{z}_u \end{bmatrix}^T \tag{4}$$

$$\dot{x} = Ax + B_1 z_r + B_2 u \tag{5}$$

$$A = \begin{bmatrix} 0 & 0 & 1 & 0 \\ 0 & 0 & 0 & 1 \\ -\frac{k_s}{m_s} & \frac{k_s}{m_s} & -\frac{b_s}{m_s} & \frac{b_s}{m_s} \\ \frac{k_s}{m_u} & -\frac{(k_s+k_t)}{m_u} & \frac{b_s}{m_u} & -\frac{b_s}{m_u} \end{bmatrix},$$

$$B_1 = \begin{bmatrix} 0 \\ 0 \\ 0 \\ \frac{k_t}{m_u} \end{bmatrix}, B_2 = \begin{bmatrix} 0 \\ 0 \\ \frac{1}{m_s} \\ -\frac{1}{m_u} \end{bmatrix} \tag{6}$$

The objective function for the LQR controller for the active suspension system is defined as (7) based on the state variables and control input. $\rho_i$ is the weight for adjusting the importance of each term in (7). The values of the weights are determined by using Bryson's rule [45]. Bryson's rule considers the maximum allowable value for each term to select the weights as given in (8). Since the first term of the objective function is the acceleration of the sprung mass, $\eta_1$ is set for the ride comfort. Therefore, the value of $\eta_1$ should be a lower value than other values of $\eta_i$. Meanwhile, the values of $\eta_2$ and $\eta_3$ for suspension stroke and tire deflection should be higher to improve the road adhesion and cornering performance. The weighting matrices, $\mathbf{Q}$, $\mathbf{N}$ and $\mathbf{R}$, are defined based on the weights given in (7). LQR is employed to design a controller in the form of full-state feedback, which minimizes $J$. Riccati equation with $\mathbf{A}$, $\mathbf{B}_2$, $\mathbf{Q}$, $\mathbf{N}$ and $\mathbf{R}$is used to calculate the gain matrix $\mathbf{K}$ for the LQR controller. As shown in (9), $\mathbf{K}$ consists of four elements, such as the number of state variables. In this paper, this controller $\mathbf{K}$ is denoted as LQRq.

$$\begin{aligned} J &= \int_0^\infty \left\{ \rho_1 \ddot{z}_s^2 + \rho_2 (z_s - z_u)^2 + \rho_3 z_u^2 + \rho_4 u^2 \right\} dt \\ &= \int_0^\infty \left\{ \begin{bmatrix} x \\ u \end{bmatrix}^T \begin{bmatrix} Q & N \\ N^T & R \end{bmatrix} \begin{bmatrix} x \\ u \end{bmatrix} \right\} dt \end{aligned} \tag{7}$$

$$\rho_i = 1/\eta_i^2, \; i = 1, 2, 3, 4 \tag{8}$$

$$u = -Kx = -\begin{bmatrix} k_1 & k_2 & k_3 & k_4 \end{bmatrix} x \tag{9}$$

If a 7-DOF full-car model is used, the controller determines 4 control inputs form 14 state variables. Hence, the gain matrix of LQR for 7-DOF full-car model is composed of 56 elements. However, it is difficult to measure or estimate 14 state variables with sensors or state estimators. Moreover, it is too difficult to implement LQR in actual vehicles. On the other hand, the controller (9) has four gain elements and requires 4 state variables to be measured or estimated. Hence, it is much easier to implement it [15], [16]. In this paper, the controller (9) is used to generate the control force, $u$. When generating the control force $u$, several types of actuators such as an active actuator and a semi-active actuator are available in actual vehicles.

## III. COORDINATED COMPENSATION SCHEMES FOR ACTIVE AND SEMI-ACTIVE ACTUATORS

Up to date, two types of actuators have been used for suspension control systems: active and semi-active actuators. An air spring can be used as an actuator for suspension control. However, it has been used mainly for height control of a sprung mass, which is not relevant to ride comfort [46].

Hence, an air spring is not considered as an actuator for suspension control in this paper.

Typical active actuators are hydraulic, electro-magnetic, and electro-mechanical ones [1], [8]. These active actuators have been commercialized in actual vehicles [47]. The benefit of these actuators is that the direction of the actuator force is independent of the sign of the actuator velocity. However, it requires a large amount of power. Generally, hydraulic actuators require a pump, control valves and power supply lines, which is expensive and too large to be installed on actual vehicles. Moreover, its energy conversion efficiency is poor. Electro-mechanical actuators such as electric motors with rack and pinion or ball-screw mechanism have force-velocity limit. Fig. 2 shows the peak and continuous capacity curves of a commercial electro-mechanical actuator, which consists of electric motor and ball screw mechanism [48]. In Fig. 2, the shaded areas represent the continuous regions, and the dotted lines do peak regions. Outside these regions, the actuator cannot generate a force. As shown in Fig. 2, the larger the speed, the smaller the maximum force. Moreover, the continuous regions are much smaller than the peak ones. The legends Type A, Type B and Type C in Fig. 2 represent the options that one can select according to a particular application. For example, the actuator Type A can generate a larger force than the others with smaller velocity limit. On the other hand, the actuator Type C can generate a smaller force with larger velocity limit.

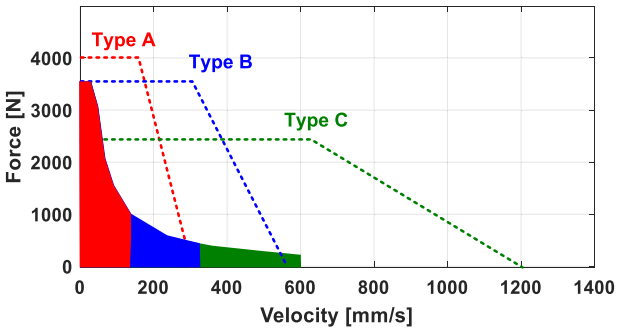


**FIGURE 2.** Peak and continuous capacity curves for each actuator type.

Typical semi-active actuators are hydraulic shock absorbers, magneto-rheological (MR), electro-rheological (ER), and electromagnetic dampers [1], [8]. Compared to active actuators, semi-active ones require smaller power and size. Moreover, it has no force-velocity limit just like an active actuator. The typical drawback of semi-active actuators is that it can generate the actuator force only in 2 and 4 quadrants on a velocity-force plane. The features of active and semi-actuators were summarized in the literature [47], [49].

Active and semi-active actuators have several physical limitations. Fig. 3 shows the control areas of active and semi-active actuators. In Fig. 3, the control area of active actuator is derived from the peak regions given in Fig. 2. As shown in Fig. 3, the maximum force that an active actuator can generate is limited to 2000N. Moreover, an electro-mechanical actuator cannot generate a control force over the suspension velocity of 1.2 m/s. On the other hand, a semi-active actuator cannot generate a control force in 1 and 3 quadrants because it can generate a resistant force by locking the movement of a suspension. However, the semi-active actuator can generate a larger control force at high velocity over 1.2 m/s than the active one, as shown in Fig. 3. As mentioned earlier, Fig. 3 shows that the common control area of the active and semi-active actuators is small. Moreover, the separated control area is much larger than the common control one. For the reason, the active and semi-active actuators can compensate the gap between the control and actuator forces.

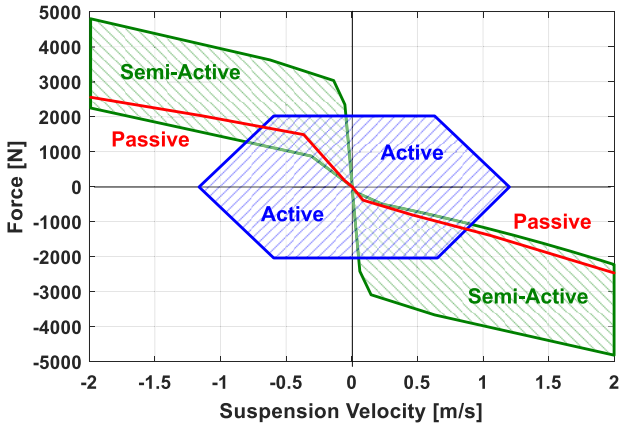


**FIGURE 3.** Effective control areas of active and semi-active actuators with respect to suspension velocity.

In this section, coordinated compensation schemes for active and semi-active actuators are proposed in order to generate the control force calculated from the controllers. Two coordinated compensation schemes, i.e., active-first and semi-active-first schemes, are proposed.

### A. ACTIVE-ONLY SCHEME

Active-only scheme is to use an active actuator to generate a control force. Fig. 4 shows the force-velocity limit of the active actuator at 1 quadrant in Fig. 3. This scheme directly apply the control input $u$ calculated from (9) under the force-velocity limit given in Figs. 3 and 4. Moreover, the active actuator has a limited bandwidth, which is modeled with first-order system, as given in (10). If an active actuator has the bandwidth of 10Hz, then $\tau$ is set to 0.01592. In (10), the constrained force $F_m$ is calculated by (11), which is derived from Fig. 4.

$$F_a = \frac{1}{\tau s + 1} \min\left(|u|, F_m\right) sgn\left(u\right) \tag{10}$$

$$F_m = \begin{cases} F_s, & |v| \le v_s \\ F_s \frac{v_z - v}{v_z - v_s}, & v_s < |v| \le v_z \\ 0, & |v| > v_z \end{cases} \tag{11}$$

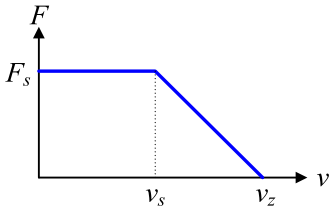


**FIGURE 4.** Force-velocity limit of an active actuator.

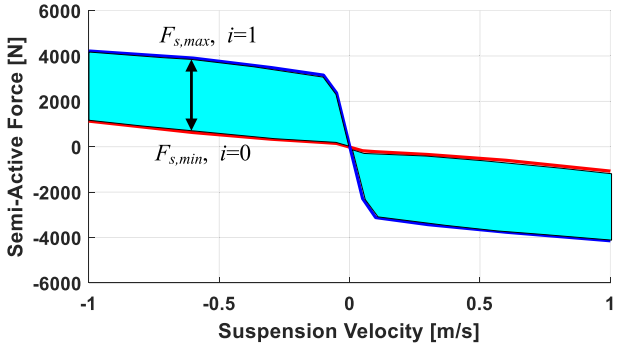


**FIGURE 5.** Characteristic curve of the semi-active actuator.

### B. SEMI-ACTIVE-ONLY SCHEME

Semi-active-first scheme is to use a semi-active actuator to generate a control force. The damping or characteristic curves of the semi-active actuator are given in Fig. 5. The input of this actuator is a current with the range from 0 to 1. As shown in Fig. 5, the normalized current 0 and 1 mean correspondingly the minimum and maximum forces that the semi-active actuator can generate at given velocity. Let denote these forces $F_{s,min}(v)$ and $F_{s,max}(v)$, respectively. The current applied to the semi-active actuator, $i_{command}$, is calculated by (12) [50]. In (12), $i_{default}$ is a damping curve, which corresponds to the passive curve in Fig. 3. The delay of this actuator is also considered. However, the hysteresis, frequency and thermal effects on the semi-active actuator are not considered [51].

$$i_{command} = \begin{cases} \frac{u - F_{s,min}(v)}{F_{s,max}(v) - F_{s,min}(v)}, & \dot{z}_s v \geq 0 \\ i_{default}, & \dot{z}_s v < 0 \end{cases} \tag{12}$$

### C. ACTIVE-FIRST SCHEME

Active-first scheme uses active and semi-active actuators simultaneously to generate a control force. In this scheme, the primary actuator is the active actuator. If the control input is inside the area of the active region given in Fig. 3, the active actuator is used alone. On the other hand, if the control force is outside the effective control areas of the active actuator, the semi-active actuator is used to compensate for the shortage of the active actuator. The additional control force $F_d$ of the semi-active actuator is defined by subtracting the active force from the control one, as given in (13). The current command to generate $F_d$ is calculated from (12) by replacing $u$ with $F_d$. This can be achieved only in 2 and 4 quadrants given in Fig. 3, because the semi-active actuator resists the movement of the suspension. Therefore, the semi-active actuator cannot assist the active actuator in 1 and 3 quadrants.

$$F_d = u - F_m \tag{13}$$

### D. SEMI-ACTIVE-FIRST SCHEME

Semi-active-first scheme also uses both actuators to generate the control force determined by the upper-level controller. However, the difference from the active first scheme is that this scheme distributes control input first to semi-active actuators. The semi-active actuator generates the control force as given in (14). The semi-active actuator generates a force as given in (12). Therefore, the active actuator is not used unless the control input exceeds the maximum force of the semi actuator in 2 and 4 quadrants. If the control input exceeds the maximum force of the semi-active actuator, the active actuator generates the additional force to satisfy the control input. If the control force is lower than the minimum force curve, the semi-active actuator exerts a minimum force. The current command for the semi-active actuator is calculated by (12). Then, the active actuator generates a control force as much as the difference between the control input and semi-active force as given in (15). The additional control input $u_a$ is applied by the active actuator. The control force of the active actuator is calculated by (10) and (11). In 1 and 3 quadrants, the semi-active actuator cannot generate a control force. However, the control force of the active actuator can be reduced by setting the semi-active actuator soft to exert only minimal damping.

$$F_d = \begin{cases} u, & \dot{z}_s v \geq 0,\ u \geq F_{s,min}(v)\, u \leq F_{s,max}(v) \\ F_{s,min}(v), & \dot{z}_s v \geq 0 u \leq F_{s,min}(v) \\ F_{s,min}(v), & \dot{z}_s v \geq 0, u \geq F_{s,max}(v) \\ F_{s,min}(v), & \dot{z}_s v < 0, \end{cases} \tag{14}$$

$$u_a = u - F_d \tag{15}$$

## IV. SIMULATION

In this section, a simulation study is conducted to evaluate the performance of two coordinated compensation schemes, i.e., active-first and semi-active-first schemes. Through a simulation, the proposed schemes are compared to each another.

The descriptions and corresponding values of the parameters for 2-DOF quarter-car model is summarized in Table 1. The parameter values are referenced from the vehicle model of Lexus NX300h given in CarMaker, named Demo_Lexus_NX300h. The maximum allowable values for the weights in the LQ objective functions are given in Table 2. The values given in Table 2 are set with ride comfort as the primary objective. In other words, the controller tries to reduce the vertical acceleration of the sprung mass while maintaining the road adhesion. Table 3 shows the controller gain matrix of LQRq.

**TABLE 1. Parameter descriptions and the corresponding values of the 2-DOF quarter-car.**

| | | |
|---|---|---|
| $m_s$ | Sprung mass of the quarter-car model | 418.0 kg |
| $m_u$ | Unsprung mass of the quarter-car model | 62.0 kg |
| $k_s$ | Spring stiffness of the quarter-car model | 35,000 N/m |
| $b_s$ | Damping coefficient of the quarter-car model | 3,500 N·s/m |
| $k_t$ | Tire stiffness of the quarter-car model | 391,961 N/m |

**TABLE 2. Maximum allowable values in LQ objective function.**

| | | | | | |
|---|---|---|---|---|---|
| $\eta_1$ | 1.0 m/s$^2$ | $\eta_2$ | 0.2 m | $\eta_3$ | 0.2 m |
| $\eta_4$ | 3,000 N | | | | |

**TABLE 3. Controller gain matrix of LQRq.**

| | |
|---|---|
| **K** | $[-28929.0 \quad 31605.0 \quad -1533.4 \quad 3019.5]$ |

### A. BUMP SIMULATION ON CARMAKER

The simulation is conducted by using the co-simulation environment with MATLAB/Simulink and IPG CarMaker, which is the vehicle simulation package. The simulation study compares four coordinate compensation schemes under disturbances of a single bump profile. The vehicle model for the simulation is Demo_Lexus_NX300h, which is one of the default vehicles provided by CarMaker. The spring and damper of the vehicle model are nonlinear. The road profile of the single bump is depicted in Fig 6. The height and length of the bump are 0.1 m and 3.6 m. The tire-road friction coefficient is set to 0.8. The initial condition of the simulation is stand-still, and the vehicle accelerates to 30 km/h using the built-in speed controller in CarMaker. After the vehicle reaches 30 km/h, the vehicle passes the bump. Since the left and right wheels of the vehicle pass the bump evenly, roll motions are negligible.

The constraints given in Fig. 3 are imposed to the active and semi-active actuators. It is also assumed that the semi-active actuator has the delay of 40ms [52]. The active actuator has the bandwidth of 10Hz, which is a realistic value compared to the previous studies that assumed a bandwidth of the active actuator as 28.6 Hz [53]. When applying the active-only scheme, a constant current was applied to the semi-active actuator. In other words, the semi-active actuator acted as a passive damper for the active-only scheme.

Fig. 7 shows the simulation results ~~and control inputs~~ for four schemes. As shown in Fig. 7, the active-first and semi-active first schemes show the best performance in terms of ride comfort. Moreover, these two schemes show nearly identical performance in terms of ride comfort. In other words, there are little differences between the active-first and semi-active-first schemes. Except the vertical acceleration, the other responses of the active-first and semi-active first schemes are nearly identical to the active-only scheme, as shown in Fig. 7. Hence, it can be concluded that the active-first and semi-active first schemes have the effect only on the vertical acceleration of the sprung mass.

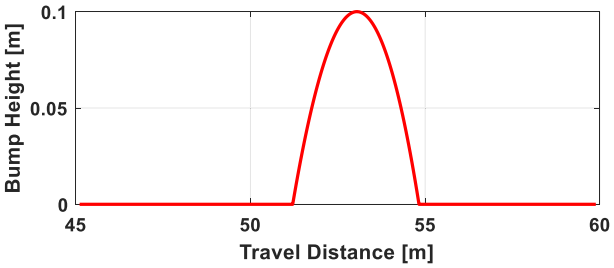


**FIGURE 6. Single bump profile.**

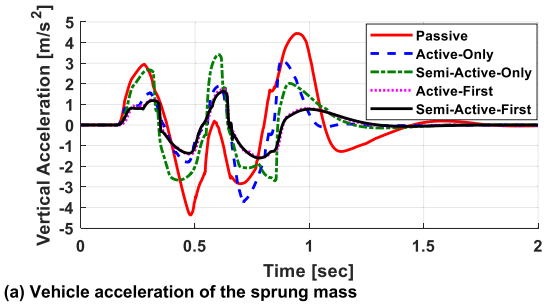


(a) Vehicle acceleration of the sprung mass

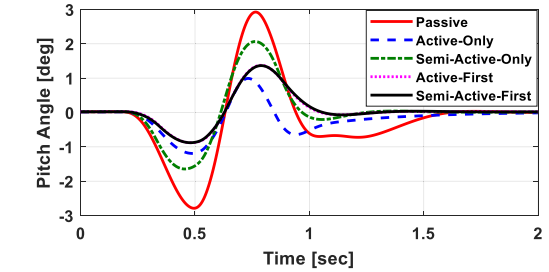


(b) Pitch angle of the sprung mass

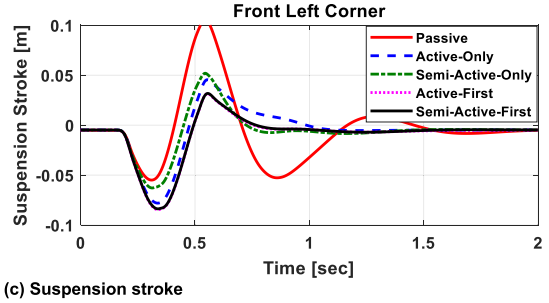


(c) Suspension stroke

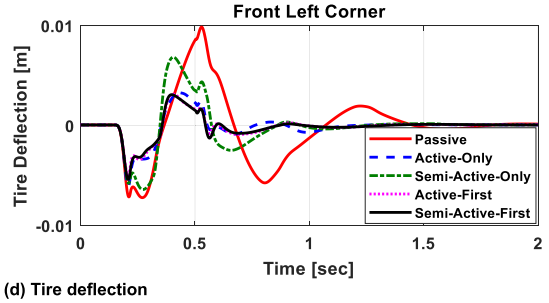


(d) Tire deflection

**FIGURE 7. Simulation results obtained from CarMaker for each controller.**

**TABLE 4.** Peak-to-peak values of responses for each controller at front left corner.

| | $\ddot{z}_c$ (m/s$^2$) | $\theta$ (deg) | SS (m) | TD (m) | Control input (N) |
|---|---|---|---|---|---|
| Passive | 8.8 | 5.7 | 0.160 | 0.017 | 0 |
| Active-only | 6.9 | 2.2 | 0.124 | 0.009 | 4294 |
| Semi-active-only | 6.1 | 3.7 | 0.115 | 0.013 | 5460 |
| Active-first | 3.3 | 2.3 | 0.116 | 0.008 | 4003 |
| Semi-active-first | 3.2 | 2.2 | 0.115 | 0.008 | 4006 |

**TABLE 5.** Root-mean-square values of responses for each controller at front left corner.

| | $\ddot{z}_c$ (m/s$^2$) | $\theta$ (deg) | SS (m) | TD (m) | Control input (N) |
|---|---|---|---|---|---|
| Passive | 0.73 | 0.49 | 0.015 | 0.001 | 0 |
| Active-only | 0.48 | 0.20 | 0.011 | 0.001 | 372 |
| Semi-active-only | 0.56 | 0.33 | 0.010 | 0.001 | 426 |
| Active-first | 0.29 | 0.21 | 0.011 | 0.001 | 351 |
| Semi-active-first | 0.28 | 0.21 | 0.011 | 0.001 | 350 |

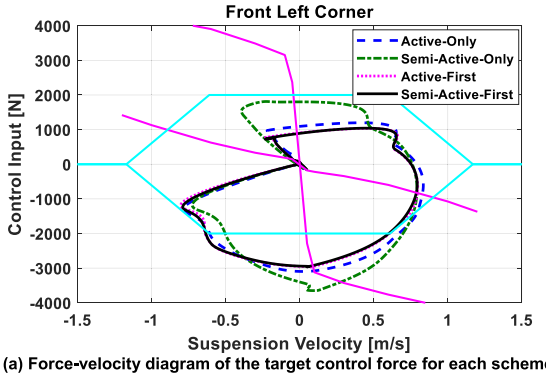

(a) Force-velocity diagram of the target control force for each scheme

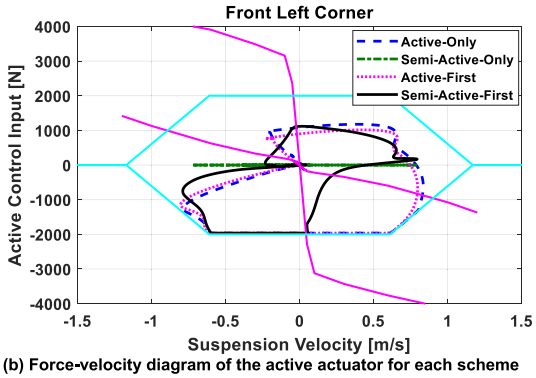

(b) Force-velocity diagram of the active actuator for each scheme

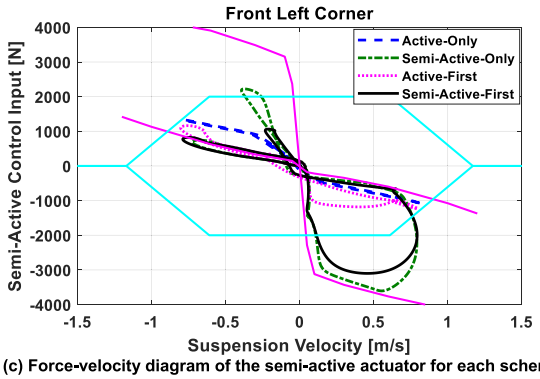

(c) Force-velocity diagram of the semi-active actuator for each scheme

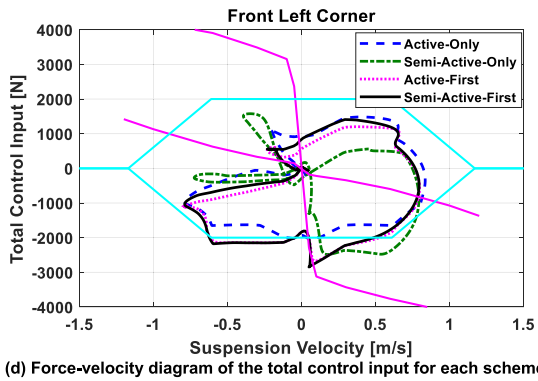

(d) Force-velocity diagram of the total control input for each scheme

**FIGURE 8.** Control inputs for each coordination scheme.

Fig. 8 shows the control inputs for four schemes. Fig. 8-(a) shows the target control forces calculated from the upper-level controller for each scheme. These are reference forces for actuators to generate. As shown in Fig. 8-(b), the control forces of the active actuator were saturated at 3 and 4 quadrants, compared to the target control forces of Fig. 8-(a). As shown in Fig. 8-(c), the control forces of the semi-active actuator cannot be generated at 2 and 4 quadrants. Fig. 8-(d) is just the sum of the control forces of the active and semi-active actuators, i.e., Figs. 8-(b) and -(c), for each scheme.

By comparing Figs. 8-(a) with -(d), the active-first and semi-active-first schemes can generate the target control force except at 3 quadrant. At 3 quadrant, the semi-active actuator cannot generate the control force. As a result, only the active actuator is available at the quadrant. However, the active actuator is saturated by the force-velocity limit. Hence, the active-first and semi-active first schemes are bound to show identical control performance at 3 quadrant.

At 4 quadrant, both of the active and semi-active actuators are available. At that quadrant, the semi-active actuator can generate the control force in spite of the saturation of the active actuator, as shown in Fig. 3. For the active-first scheme, the semi-active actuator can cover the lack of the control force caused by the saturation of the active actuator. For the semi-active scheme, the active actuator don't have to generate much less control force because the semi-active actuator can generate much larger control force.

In summary, the active-first and semi-active-first schemes can generate the target control force except at 3 quadrant, as shown in Fig. 8-(a) and -(d). As a consequence, the control performance of these two schemes is nearly identical to each other. In general, an active actuator requires more actuation energy than the semi-active one. Hence, it is desirable to use the semi-active-first scheme instead of the active-first one.

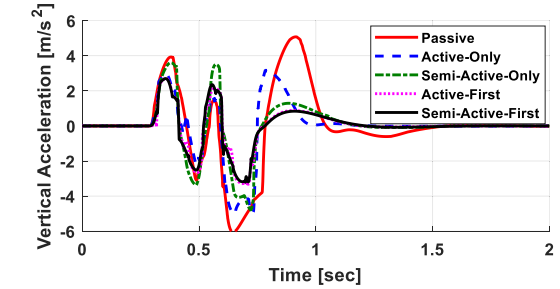


(a) Vehicle acceleration of the sprung mass

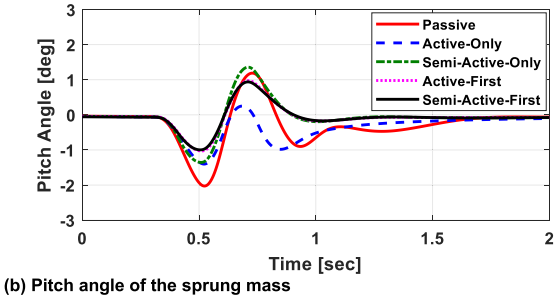


(b) Pitch angle of the sprung mass

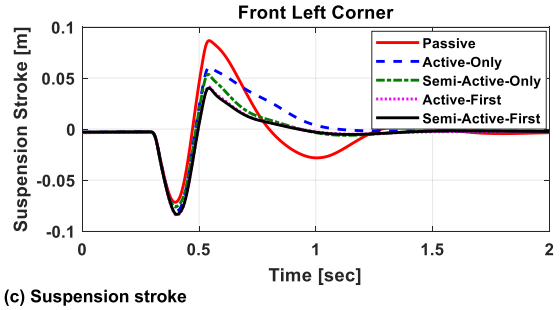


(c) Suspension stroke

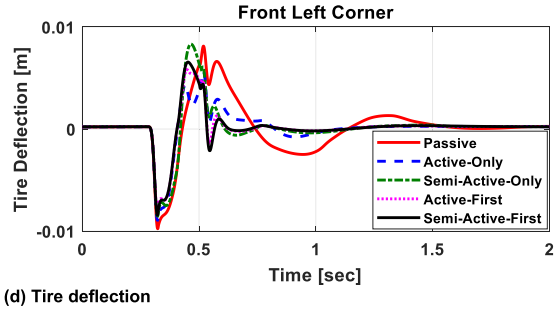


(d) Tire deflection

**FIGURE 9.** Simulation results obtained from carmaker for each controller.

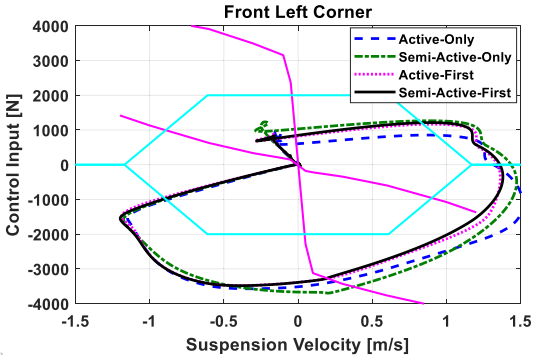


(a) Force-velocity diagram of the control force for each scheme

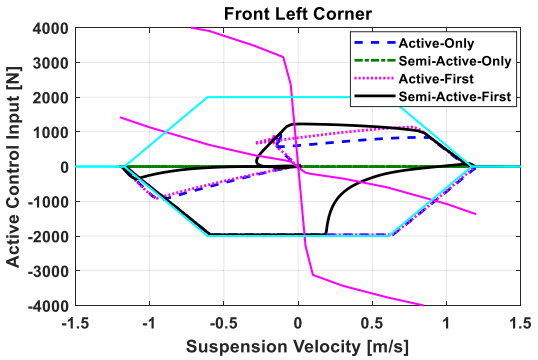


(b) Force-velocity diagram of the active actuator for each scheme

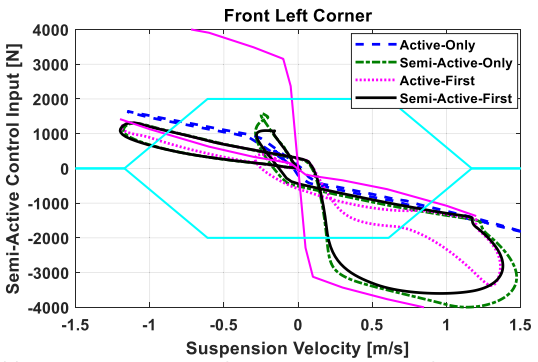


(c) Force-velocity diagram of the semi-active actuator for each scheme

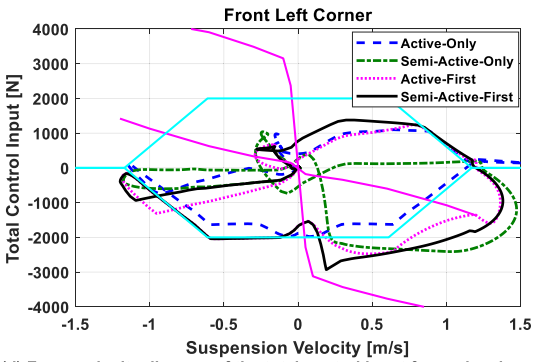


(d) Force-velocity diagram of the total control input for each scheme

**FIGURE 10.** Control inputs for each coordination scheme.

Tables 4 and 5 show the peak-to-peak and root-mean-square values of the responses shown in Figs. 7 and 8 for each scheme. In Tables 4 and 5, SS is the suspension stroke and TD is the tire deflection. The maximum absolute values of the measures given in Table 4 can be calculated as half of the corresponding values. As shown in Tables 4 and 5, the vertical acceleration of the active-first and semi-active-first schemes decreased, compared to the active-only and the semi-active-only. For instance from Table 4, the vertical accelerations of the sprung mass with the active-first and semi-active-first schemes are reduced to 38%, 48% and 54% of the passive, active-only and semi-active-only schemes, respectively. These results show that the active-first and semi-active-first schemes have the effect only on the vertical acceleration of the sprung mass. All values of the active-first and semi-active-first schemes are nearly identical to each other. Especially, the control inputs of these two schemes, i.e., 4003 and 4006 in

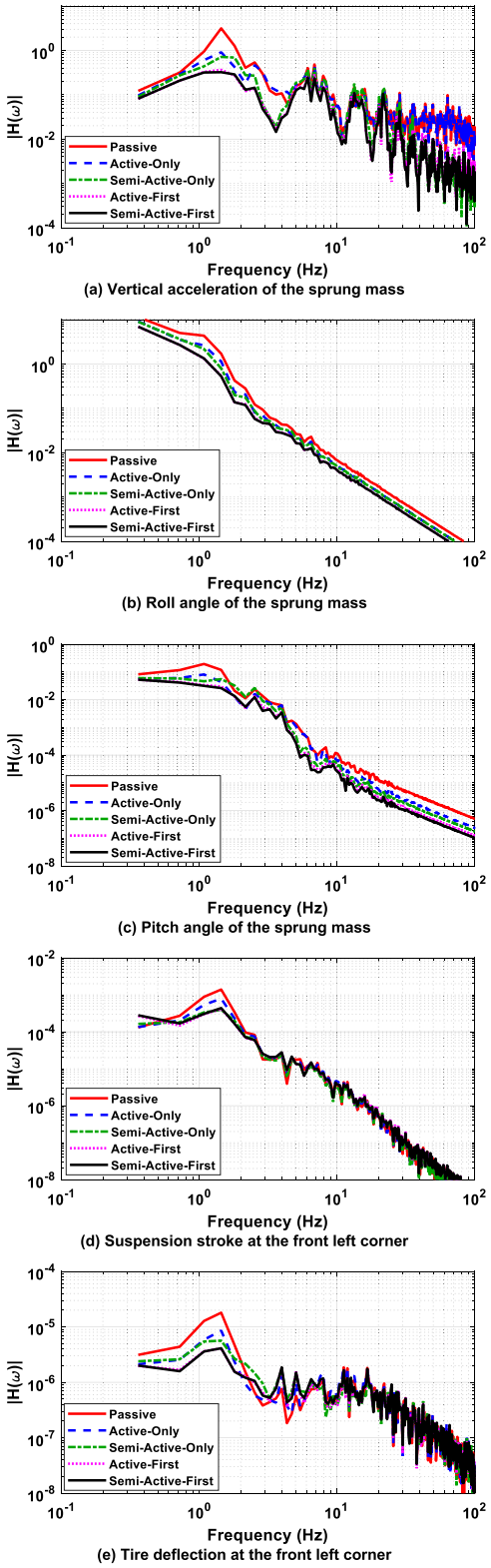


**FIGURE 11. Frequency responses of coordination schemes on ISO random roads.**

Table 4, are almost identical. This fact means that these two schemes can fully generate the control force, generated from the upper-level controller. As shown in Table 4, the semi-active actuator can reduce the suspension stroke, compared to the active one. This feature holds for the active-first and the semi-active-first schemes.

To check the effects of the proposed schemes on control performance, a simulation was conducted at higher speed, i.e., 50km/h. The simulation conditions were identical to those of the previous one except the vehicle speed. Figs. 9 and 10 show the simulation results and the control inputs for the case that the vehicle speed was set to 50km/h. As shown in Fig. 9, the vertical accelerations increase, compared to those of Fig. 7. Nevertheless, same as the results in Fig. 7, the active-first and semi-active-first schemes show the best performance in controlling the vertical acceleration. Moreover, these two schemes nearly identical performance in terms of ride comfort. This was expected that the proposed coordination schemes can generate the control force calculated from the upper-level controller because the semi-active actuator can generate much larger control force in spite of the saturation of the active actuator. This fact can be checked at Figs. 10-(a) and -(d). The difference between the results of Figs. 8 and 10 is that the active actuator was saturated at 1 quadrant, as shown in Fig. 10-(b) and -(d). This is caused by the fact that the semi-active actuator is not available at 1 quadrant. As a result, none of four schemes cannot generate the target control force at that quadrant.

Fig. 11 shows the simulations results of the proposed coordination schemes on ISO random road with level D form the CarMaker simulation [54]. The simulation was done with the four coordinate compensation schemes under the condition that the vehicle speed is set to 30km/h. Frequency responses obtained from the CarMaker simulation are described in Fig. 11 for each scheme on the ISO random road profile with level D. As shown in Fig. 11, the active-first and semi-active-first schemes show the best performance in terms of ride comfort. As given in Fig. 7, Tables 4 and 5, these two schemes show almost identical performance in ride comfort. Notable feature is that the semi-active-first scheme shows better performance at the high frequency over 10Hz, as given in Fig. 11-(a). This is expected from the feature of the semi-active actuator [49].

## V. CONCLUSION

In this paper, two coordinated compensation schemes were proposed for the suspension control system that simultaneously uses active and semi-active actuators. Based on the physical constraints such as saturation and force-velocity limit of the active and semi-actuators, the proposed schemes compensate the drawbacks of two actuators. Through a simulation done on the vehicle simulation package, CarMaker, it can be concluded that the coordinated compensation schemes, i.e., the active-first and semi-active-first schemes, have the effect only on the vertical acceleration of the sprung mass. It is also checked that the semi-active actuator is effective in controlling the vertical motion of the sprung mass at high frequency over 10Hz, which has been well known. In terms of the control input of each actuator, it is desirable

to use the active actuator for suspension control because it requires small assist force of the semi-active actuator when reducing the vertical acceleration of the sprung mass. Further research can include experiments on actual devices or actual vehicles and investigation into parameter sensitivity of the active and semi-active actuators on the control performance.

## REFERENCES

[1] H. E. Tseng and D. Hrovat, "State of the art survey: Active and semi-active suspension control," *Vehicle Syst. Dyn.*, vol. 53, no. 7, pp. 1034–1062, 2015, doi: 10.1080/00423114.2015.1037313.

[2] *Mechanical Vibration and Shock—Evaluation of Human Exposure to Whole-Body Vibration—Part 1: General Requirements*, Standard ISO 2631-1, International Organization for Standardization, Geneva, Switzerland, 1997.

[3] A. N. Rimell and N. J. Mansfield, "Design of digital filters for frequency weightings required for risk assessments of workers exposed to vibration," *Ind. Health*, vol. 45, no. 4, pp. 512–519, 2007, doi: 10.2486/indhealth.45.512.

[4] T. Tseng and D. Hrovat, "Some characteristics of optimal vehicle suspensions based on quarter-car models," in *Proc. 29th IEEE Conf. Decis. Control*, Dec. 1990, pp. 2232–2237, doi: 10.1109/CDC.1990.204022.

[5] D. Hrovat, "Survey of advanced suspension developments and related optimal control applications," *Automatica*, vol. 33, no. 10, pp. 1781–1817, 1997, doi: 10.1016/S0005-1098(97)00101-5.

[6] D. Cao, X. Song, and M. Ahmadian, "Editors' perspectives: Road vehicle suspension design, dynamics, and control," *Vehicle Syst. Dyn.*, vol. 49, nos. 1–2, pp. 3–28, Feb. 2011, doi: 10.1080/00423114.2010.532223.

[7] C. Poussot-Vassal, C. Spelta, O. Sename, S. M. Savaresi, and L. Dugard, "Survey and performance evaluation on some automotive semi-active suspension control methods: A comparative study on a single-corner model," *Annu. Rev. Control*, vol. 36, no. 1, pp. 148–160, Apr. 2012, doi: 10.1016/j.arcontrol.2012.03.011.

[8] J. Theunissen, A. Tota, P. Gruber, M. Dhaens, and A. Sorniotti, "Preview-based techniques for vehicle suspension control: A state-of-the-art review," *Annu. Rev. Control*, vol. 51, pp. 206–235, Jan. 2021, doi: 10.1016/j.arcontrol.2021.03.010.

[9] A. Soliman and M. Kaldas, "Semi-active suspension systems from research to mass-market—A review," *J. Low Freq. Noise, Vibrat. Act. Control*, vol. 40, no. 2, pp. 1005–1023, Jun. 2021, doi: 10.1177/1461348419876392.

[10] K. J. Waldron and M. E. Abdallah, "An optimal traction control scheme for off-road operation of robotic vehicles," *IEEE/ASME Trans. Mechatronics*, vol. 12, no. 2, pp. 126–133, Apr. 2007, doi: 10.1109/TMECH.2007.892819.

[11] J. Nah and S. Yim, "Vehicle stability control with four-wheel independent braking, drive and steering on in-wheel motor-driven electric vehicles," *Electronics*, vol. 9, no. 11, p. 1934, Nov. 2020, doi: 10.3390/electronics9111934.

[12] M. Yu, C. Arana, S. A. Evangelou, D. Dini, and G. D. Cleaver, "Parallel active link suspension: A quarter-car experimental study," *IEEE/ASME Trans. Mechatronics*, vol. 23, no. 5, pp. 2066–2077, Oct. 2018, 10.1109/TMECH.2018.2864785.

[13] T. A. Johansen and T. I. Fossen, "Control allocation—A survey," *Automatica*, vol. 49, no. 5, pp. 1087–1103, 2013, doi: 10.1016/j.automatica.2013.01.035.

[14] T. Attia, K. G. Vamvoudakis, K. Kochersberger, J. Bird, and T. Furukawa, "Simultaneous dynamic system estimation and optimal control of vehicle active suspension," *Vehicle Syst. Dyn.*, vol. 57, no. 10, pp. 1467–1493, Oct. 2019, doi: 10.1080/00423114.2018.1521000.

[15] M. Park and S. Yim, "Design of static output feedback and structured controllers for active suspension with quarter-car model," *Energies*, vol. 14, no. 24, p. 8231, Dec. 2021, doi: 10.3390/en14248231.

[16] Y. Jeong, Y. Sohn, S. Chang, and S. Yim, "Design of static output feedback controllers for an active suspension system," *IEEE Access*, vol. 10, pp. 26948–26964, 2022, doi: 10.1109/ACCESS.2022.3157326.

[17] M. Yang, C. Peng, G. Li, Y. Wang, and S. Ma, "Event-triggered $H_\infty$ control for active semi-vehicle suspension system with communication constraints," *Inf. Sci.*, vol. 486, pp. 101–113, Jun. 2019, doi: 10.1016/j.ins.2019.02.047.

[18] Y. Zhang, M. Liu, and C. Zhang, "Robust fault-tolerant $H_\infty$ output feedback control of active suspension and dynamic vibration absorber with finite-frequency constraint," *IET Intell. Transp. Syst.*, vol. 14, no. 14, pp. 1935–1945, Dec. 2020, doi: 10.1049/iet-its.2020.0364.

[19] H. Du and N. Zhang, "Fuzzy control for nonlinear uncertain electrohydraulic active suspensions with input constraint," *IEEE Trans. Fuzzy Syst.*, vol. 17, no. 2, pp. 343–356, Apr. 2009, doi: 10.1109/TFUZZ.2008.2011814.

[20] A. S. Gad, H. El-Zoghby, W. Oraby, and S. M. M. El-Demerdash, "Application of a preview control with an MR damper model using genetic algorithm in semi-active automobile suspension," SAE Tech. Paper 2019-01-5006, 2019, doi: 10.4271/2019-01-5006.

[21] Y. Huang, J. Na, X. Wu, X. Liu, and Y. Guo, "Adaptive control of nonlinear uncertain active suspension systems with prescribed performance," *ISA Trans.*, vol. 54, pp. 145–155, Jan. 2015, doi: 10.1016/j.isatra.2014.05.025.

[22] H. Pan, W. Sun, X. Jing, H. Gao, and J. Yao, "Adaptive tracking control for active suspension systems with non-ideal actuators," *J. Sound Vibrat.*, vol. 399, pp. 2–20, Jul. 2017, doi: 10.1016/j.jsv.2017.03.011.

[23] X. Su, "Master–slave control for active suspension systems with hydraulic actuator dynamics," *IEEE Access*, vol. 5, pp. 3612–3621, 2017, doi: 10.1109/ACCESS.2017.2672598.

[24] L. Liu, C. Zhu, Y.-J. Liu, R. Wang, and S. Tong, "Performance improvement of active suspension constrained system via neural network identification," *IEEE Trans. Neural Netw. Learn. Syst.*, early access, Jan. 1, 2022, doi: 10.1109/TNNLS.2021.3137883.

[25] Y. Liu and L. Zuo, "Energy-flow-driven (EFD) semi-active suspension control," in *Proc. Amer. Control Conf.*, Portland, OR, USA, Jun. 2014, pp. 4–6, doi: 10.1109/ACC.2014.6859282.

[26] E. Enders, G. Burkhard, and N. Munzinger, "Analysis of the influence of suspension actuator limitations on ride comfort in passenger cars using model predictive control," *Actuators*, vol. 9, no. 3, p. 77, Aug. 2020, doi: 10.3390/act9030077.

[27] M. A. Karkoub and M. Zribi, "Active/semi-active suspension control using magnetorheological actuators," *Int. J. Syst. Sci.*, vol. 37, no. 1, pp. 35–44, Jan. 2006, doi: 10.1080/00207720500436344.

[28] K. El Majdoub, D. Ghani, F. Giri, and F. Z. Chaoui, "Adaptive semi-active suspension of quarter-vehicle with magnetorheological damper," *J. Dyn. Syst., Meas., Control*, vol. 137, no. 2, Feb. 2015, Art. no. 021010, doi: 10.1115/1.4028314.

[29] S. Kilicaslan, "Control of active suspension system considering nonlinear actuator dynamics," *Nonlinear Dyn.*, vol. 91, no. 2, pp. 1383–1394, 2018, doi: 10.1007/s11071-017-3951-x.

[30] Y. Qin, J. J. Rath, C. Hu, C. Sentouh, and R. Wang, "Adaptive nonlinear active suspension control based on a robust road classifier with a modified super-twisting algorithm," *Nonlinear Dyn.*, vol. 97, no. 4, pp. 2425–2442, Sep. 2019, doi: 10.1007/s11071-019-05138-8.

[31] X. Shao, F. Naghdy, H. Du, and Y. Qin, "Coupling effect between road excitation and an in-wheel switched reluctance motor on vehicle ride comfort and active suspension control," *J. Sound Vibrat.*, vol. 443, pp. 683–702, Mar. 2019, doi: 10.1016/j.jsv.2018.12.012.

[32] X. Shao, F. Naghdy, H. Du, and H. Li, "Output feedback $H_\infty$ control for active suspension of in-wheel motor driven electric vehicle with control faults and input delay," *ISA Trans.*, vol. 92, pp. 94–108, Sep. 2019, doi: 10.1016/j.isatra.2019.02.016.

[33] T. P. J. van der Sande, B. L. J. Gysen, I. J. M. Besselink, J. J. H. Paulides, E. A. Lomonova, and H. Nijmeijer, "Robust control of an electromagnetic active suspension system: Simulations and measurements," *Mechatronics*, vol. 23, no. 2, pp. 204–212, Mar. 2013, doi: 10.1016/j.mechatronics.2012.07.002.

[34] S. Nie, Y. Zhuang, W. Liu, and F. Chen, "A semi-active suspension control algorithm for vehicle comprehensive vertical dynamics performance," *Vehicle Syst. Dyn.*, vol. 55, no. 8, pp. 1099–1122, Aug. 2017, doi: 10.1080/00423114.2017.1299871.

[35] M. Yu, C. Arana, S. A. Evangelou, and D. Dini, "Quarter-car experimental study for series active variable geometry suspension," *IEEE Trans. Control Syst. Technol.*, vol. 27, no. 2, pp. 743–759, Mar. 2019, doi: 10.1109/TCST.2017.2772912.

[36] M. M. Morato, M. Q. Nguyen, O. Sename, and L. Dugard, "Design of a fast real-time LPV model predictive control system for semi-active suspension control of a full vehicle," *J. Franklin Inst.*, vol. 356, no. 3, pp. 1196–1224, Feb. 2019, doi: 10.1016/j.jfranklin.2018.11.016.

[37] R. Wang, W. Liu, R. Ding, X. Meng, Z. Sun, L. Yang, and D. Sun, "Switching control of semi-active suspension based on road profile estimation," *Vehicle Syst. Dyn.*, vol. 2021, pp. 1–21, Feb. 2021, doi: 10.1080/00423114.2021.1889621.

[38] J. Na, Y. Huang, X. Wu, Y.-J. Liu, Y. Li, and G. Li, "Active suspension control of quarter-car system with experimental validation," *IEEE Trans. Syst., Man, Cybern. Syst.*, early access, Sep. 6, 2021, doi: 10.1109/TSMC.2021.3103807.

[39] G. Koch, O. Fritsch, and B. Lohmann, "Potential of low bandwidth active suspension control with continuously variable damper," *Control Eng. Pract.*, vol. 18, no. 11, pp. 1251–1262, Nov. 2010, doi: 10.1016/j.conengprac.2010.03.007.

[40] M. K. Binder and A. Khajepour, "Optimal control allocation for coordinated suspension control," in *Proc. Amer. Control Conf.*, Portland, OR, USA, Jun. 2014, pp. 4–6, doi: 10.1109/ACC.2014.6859119.

[41] J. N. Strohm and B. Lohmann, "A fast convergence FxLMS algorithm for vibration damping of a quarter car," in *Proc. IEEE Conf. Decis. Control*, Miami Beach, FL, USA, Dec. 2018, pp. 6094–6100, doi: 10.1109/CDC.2018.8619688.

[42] J. N. Strohm and F. Christ, "Preview $H_\infty$ control of a hybrid suspension system," *IFAC-PapersOnLine*, vol. 52, no. 5, pp. 237–242, 2019, doi: 10.1016/j.ifacol.2019.09.038.

[43] R. Ding, R. Wang, X. Meng, and L. Chen, "Energy consumption sensitivity analysis and energy-reduction control of hybrid electromagnetic active suspension," *Mech. Syst. Signal Process.*, vol. 134, Dec. 2019, Art. no. 106301, doi: 10.1016/j.ymssp.2019.106301.

[44] D. Ning, S. Sun, H. Du, and W. Li, "Integrated active and semi-active control for seat suspension of a heavy duty vehicle," *J. Intell. Mater. Syst. Struct.*, vol. 29, no. 1, pp. 91–100, Jan. 2018, doi: 10.1177/1045389X17721032.

[45] A. E. Bryson and Y. Ho, *Applied Optimal Control*. New York, NY, USA: Taylor & Francis Group, 1975, p. 149, doi: 10.1201/9781315137667.

[46] H. Qi, Y. Chen, N. Zhang, B. Zhang, D. Wang, and B. Tan, "Improvement of both handling stability and ride comfort of a vehicle via coupled hydraulically interconnected suspension and electronic controlled air spring," *Proc. Inst. Mech. Eng., D, J. Automobile Eng.*, vol. 234, nos. 2–3, pp. 552–571, Feb. 2019, doi: 10.1177/0954407019856538.

[47] X. D. Xue, K. W. E. Cheng, Z. Zhang, J. K. Lin, D. H. Wang, Y. J. Bao, M. K. Wong, and N. Cheung, "Study of art of automotive active suspensions," in *Proc. 4th Int. Conf. Power Electron. Syst. Appl.*, Hong Kong, Jun. 2011, pp. 8–10, doi: 10.1109/PESA.2011.5982958.

[48] Tolomatic. *IMA Integrated Motor Rod-Style Actuator User Manual—2700-4001 IMA Integrated Motor Rod-Style Actuator*. Accessed: Mar. 25, 2022. [Online]. Available: https://www.tolomatic.com/info-center/resource-details/ima-integrated-motor-rod-style-actuator-user-manual

[49] L. BalaMurugan and J. Jancirani, "An investigation on semi-active suspension damper and control strategies for vehicle ride comfort and road holding," *Proc. Inst. Mech. Eng., I, J. Syst. Control Eng.*, vol. 226, no. 8, pp. 1119–1129, Sep. 2012, doi: 10.1177/0959651812447520.

[50] S. Yim, "Active roll stabilization with disturbance feedforward control," *IEEE Access*, vol. 9, pp. 19788–19799, 2021, doi: 10.1109/ACCESS.2021.3054837.

[51] D. Guo and H. Hu, "Nonlinear stiffness of a magneto-rheological damper," *Nonlinear Dyn.*, vol. 40, no. 3, pp. 241–249, May 2005, doi: 10.1007/s11071-005-6464-y.

[52] C. A. Vivas-Lopez, D. Hernández-Alcántara, M. Q. Nguyen, R. Morales-Menendez, and O. Sename, "Force control system for an automotive semi-active suspension," *IFAC-PapersOnLine*, vol. 48, no. 26, pp. 55–60, 2015, doi: 10.1016/j.ifacol.2015.11.113.

[53] G. Koch and T. Kloiber, "Driving state adaptive control of an active vehicle suspension system," *IEEE Trans. Control Syst. Technol.*, vol. 22, no. 1, pp. 44–57, Jan. 2013, doi: 10.1109/TCST.2013.2240455.

[54] P. Múčka, "Simulated road profiles according to ISO 8608 in vibration analysis," *J. Test. Eval.*, vol. 46, no. 1, pp. 405–418, 2018, doi: 10.1520/JTE20160265.

**YONGHWAN JEONG** received the B.S. and Ph.D. degrees in mechanical engineering from Seoul National University, South Korea, in 2014 and 2020, respectively. From 2020 to 2021, he was a Senior Research Engineer with Hyundai Motor Company, South Korea. Since 2021, he has been an Assistant Professor with the Department of Mechanical and Automotive Engineering, Seoul National University of Science and Technology, South Korea. His research interests include sensor fusion with vehicular communication, risk assessment, driver intention inference with trajectory prediction, motion planning, and control of urban automated vehicle.

**YOUNGIL SOHN** received the B.S. and M.S. degrees in mechanical engineering from the Korea Advanced Institute of Science and Technology (KAIST), South Korea, in 1994 and 1996, respectively. From 1996 to 2012, he was a Principal Research Engineer with the Institute for Advanced Engineering (IAE), South Korea. From 2012 to 2021, he was a Senior Research Engineer with the Research and Development Center, Hyundai Motor Company, South Korea, where he has been working as a Senior Research Engineer with the Institute of Advanced Technology Development (IATD), since 2021. His research interests include control software development for semi-active and active suspension for vehicle ride comfort, and artificial intelligent application for vehicle chassis control.

**SEHYUN CHANG** received the B.S. degree from Korea Aerospace University, South Korea, in 1996, the M.S. degree in aeronautical engineering from Seoul National University, South Korea, in 1998, and the Ph.D. degree in mechanical engineering from the University of Michigan, Ann Arbor, in 2007. Since 2007, he has been a Senior Research Engineer at the Research and Development Center, Hyundai Motor Company, South Korea. His research interests include vehicle dynamics, integrated chassis control, model predictive control, future mobility, and design optimization,

**SEONGJIN YIM** (Member, IEEE) received the B.S. degree in mechanical engineering from Yonsei University, South Korea, in 1995, and the M.S. and Ph.D. degrees in mechanical engineering from the Korea Advanced Institute of Science and Technology (KAIST), in 1997 and 2007, respectively.

From 2008 to 2010, he was a Postdoctoral Researcher with the BK21 School for Creative Engineering Design of Next Generation Mechanical and Aerospace Systems, Seoul National University. From 2011 to 2013, he was a Research Professor with the Advanced Institutes of Convergence Technology, Seoul National University. Since 2019, he has been an Associate Professor with the Department of Mechanical and Automotive Engineering, Seoul National University of Science and Technology, South Korea. His research interests include autonomous driving, integrated chassis control systems with V2V communication, cloud computing-based vehicle control, and active suspension control.